Primary and Secondary Hydration Forces between Interdigitated Membranes Composed of Bolaform Microbial Glucolipids

Niki Baccile, Viviana Cristiglio

Primary and Secondary Hydration Forces between Interdigitated Membranes Composed of Bolaform Microbial Glucolipids

Niki Baccile,[a*] Viviana Cristiglio,[b] Bruno Demé,[b]

[a] Sorbonne Université, Centre National de la Recherche Scientifique, Laboratoire de Chimie de la Matière Condensée de Paris, LCMCP, F-75005 Paris, France

[b] Institut Laue-Langevin, 71 Avenue des Martyrs, 38042 Grenoble Cedex 9, France

Abstract

To better understand lipid membranes in living organisms, the study of intermolecular forces using the osmotic pressure technique applied to model lipid membranes has constituted the ground knowledge in the field since four decades. However, the study of intermolecular forces in lipid systems other than phospholipids, like glycolipids, has gained a certain interest only recently. Even in this case, the work generally focus on the study of membrane glycolipids, but little is known on new forms of non-membrane functional compounds, like pH-responsive bolaform glycolipids. This works explores, through the osmotic stress method involving an adiabatic humidity chamber coupled to neutron diffraction, the short-range (< 2 nm) intermolecular forces of membranes entirely composed of interdigitated glucolipids. Experiments are performed at pH 6, when the glucolipid is partially negatively charged and for which we explore the effect of low (16 mM) and high (100 mM) ionic strength. We find that this system is characterized by primary and secondary hydration regimes, respectively insensitive and sensitive to ionic strength and with typical decay lengths of λ_{H1}= 0.37 ± 0.12 nm and λ_{H2}=1.97 ± 0.78 nm.

Introduction

Understanding the physical properties of biological membranes has long been a goal in biophysics and colloid science.[1–3] Due to their complex composition and the evident difficulties to study them *in-vivo*,[1] research is generally focused on the simplification of complexity by studying intermolecular forces in model lipid systems, and exploring both structural (electrical charges, bilayer flexibility, polar headgroup composition) and physicochemical (ionic strength, pH, temperature) parameters in both neutral and charged but also mixed compositions of neutral and charged phospholipids.[1,4–11]

Interactions in lipid lamellar phases are governed by a balance between attractive and repulsive forces.[12] Van der Waals attraction is counterbalanced by short- (< ~ 2 nm)[13] and long-range (> ~2 nm) repulsive forces,[5,14,15] where steric and hydration forces are typical short-range interactions while electrostatic and entropic (undulation) forces are most common at longer distances. To this regard, osmotic stress experiments are typically employed to obtain pressure-distance profiles,[7,9,16–20] which can be faced to both classical DLVO theory and its deviations describing intermolecular forces and colloidal interactions.[5,11,13,21] Agreement or deviation between experimental pressure-distance profiles contribute, in the end, to better understand a model systems and extrapolate to living organisms.[5,10,13,19,22,23]

More recently, the quest of model lipid systems has drawn its attention away from classical phospholipids in profit of lipids characterized by a glycosylated headgroup, whereas glycolipids are minor but important components of biological membranes.[4,20,24] To this regard, the understanding of molecular interactions in glycolipid membranes is still in its infancy, because of the interesting hydration properties of sugars[25] and the broad variety of glycosidic headgroups. Stepping out of model lipid systems, a new class of entirely biobased compounds produced by microbial fermentation and characterized by a sugar headgroup, an aliphatic chain and a carboxylic acid end-group is gaining a large interest for its biobased origin, low cytotoxicity and potential applications as green amphiphiles.[26,27] These bolaform microbial glycolipids have an unpredictable, although rich, phase diagramme, characterized by the molecular sensitivity to pH, which controls the carboxylic/carboxylate, $COOH/COO^-$, ratio and, consequently, the electrostatic interactions.[28–30] In a recent series of works, we have shown the ability of a single glucose bolaform lipid to form membranes in water at pH below 7 and composed of an interdigitated lipid structure.[30–32]

This work aims at studying, for the first time, the short-range molecular interactions of a bolaform glucolipid obtained by microbial fermentation, characterized by a single glucose moiety, a C18:0 chain and an end COOH group (GC18:0). This compound is known to self-

assemble at acidic pH into an interdigitated lipid $P_{\beta,i}$ lamellar phase forming highly viscous/hydrogel solutions in water at concentrations above 1 wt% and T < 30°C.[32] Under typical conditions in bulk (C = 1-5 wt%, pH = 6-7, [NaCl] = 10-100 mM), the lamellar period at room temperature varies between 25 and 15 nm.[32]

We employ the osmotic stress technique inside an adiabatic humidity chamber[8,33] to draw pressure-distance profiles in the distance range below 2 nm and from which steric and hydration forces can be classically looked at. An adiabatic humidity chamber provides an environment where the interlamellar spacing, $d_{(100)}$, can be controlled through relative humidity inside the chamber and easily adaptable to probe the interlamellar distance by using X-ray or neutron diffraction, the latter employed in this work. At high $RH\%$, the lamellar phase is hydrated and the thickness of the water bilayer increases, generally above 2 nm, after which long-range forces, like electrostatic repulsion, overwhelms Van der Waals attraction. At low $RH\%$, the intramembrane volume decreases as a result of dehydration, and Van der Waals attraction overwhelms electrostatic repulsion, pushing the lamellae together. On the contrary, short-range (< 1 nm) repulsive interactions in lamellar systems generally contain steric and hydration components counterbalancing the Van der Waals forces. Establishing a pressure-distance relationship, $\Pi(d_w)$, with Π being the osmotic pressure and d_w the interlamellar water thickness, we will determine the nature, strength and decay length of the short ranges forces.

Materials and methods

Products. Acidic deacetylated C18:0 glucolipids (GC18:0) have been used from previously existing batch samples, the preparation and characterization (^{1}H NMR, HPLC) of which is published elsewhere.[31] Acid (HCl 37%) and base (NaOH) are purchased at Aldrich. MilliQ-quality water has been employed throughout the experimental process.

Preparation of hydrogels. Protocol of preparation and characterization of the lamellar phase from GC18:0 are reported elsewhere[32] and were adapted for this work. GC18:0 sample is dispersed in water, followed by sonication and adjustment of pH to the desired value and ionic strength. We prepared two solutions of C= 1 wt% in D_2O at pH = 6.2 and at [NaCl] = 16 mM and 100 mM. The pH is adjusted by using 1-5 µL of NaOH 1 M (0.1 M can also be used for refinement). The mixture is then sonicated between 15 and 20 min in a classical sonicating bath to reduce the size of the aggregated powder and until obtaining a homogenous, viscous, dispersion. To this solution, the desired volume of NaCl is added so to obtain a given total [Na^+]

(= [NaOH] + [NaCl]) molar concentration. To keep the dilution factor negligible, we have used a 5 M concentrated solution of NaCl. The mixture is then sonicated again during 15 min to 20 min and eventually vortexed two or three times during 15 s each. The solution can then be left at rest during 15 min to 30 min. The solution is highly viscous and it forms a gel at rest and it presents shear-thinning properties. The lamellar phase was thoroughly characterized with neutron scattering[32] before depositing on a substrate for the adiabatic desiccation experiments.

Adiabatic desiccation experiments using a humidity chamber. The GC18:0 solutions are dispersed on two separate 5 cm x 2 cm silicon wafers by simple drop cast (volume dropped: 500 μL). To enhance homogeneous spreading of the solution onto the substrate, we have used a horizontal support levelled with a 2D spirit level. The silicon substrates were let dry in an oven at 40°C until a homogeneous coating was obtained. The samples were then introduced within a pressure chamber,[34] provided at the beamline, and set under vacuum at T= 25°C. The temperature of the D_2O water bath below the sample was modified to set chamber at the desired $RH\%$ value. The sample at [NaCl]= 16 mM was let equilibrating at 98 $RH\%$ before studying, where relative humidity was lowered. The sample at [NaCl]= 100 mM sample was let equilibrating at 10 $RH\%$ and humidity was then increased.

Neutron diffraction: neutron diffraction experiments were carried out as described in ref. 47 on the D16 instrument at the Institut Laue-Langevin (ILL; Grenoble, France), using a wavelength λ= 4.5 Å (Δλ/λ= 0.01) and a sample-to-detector distance of 900 mm.[35] The focusing option provided by the vertically focusing graphite monochromator was used to maximize the incident neutron flux at the sample. The intensity of the diffracted beam was recorded by the millimeter-resolution large-area neutron detector (MILAND) ^{3}He position-sensitive detector, which consists of 320 × 320 *xy* channels with a resolution of 1 × 1 mm^2. Data analysis was performed using the ILL in-house LAMP software (www.ill.eu/instruments-support/computing-for-science/cs-software/all-software/lamp).[36] The lamellar spacing $d_{(100)}$ was obtained by a fitting the (100) peak position with a Gaussian profile. The classical I vs 2θ profile for each $RH\%$ is obtained by summarizing each integrated 2D image measured at a given value of omega. Intensities on the detector surface were corrected for solid angle and pixel efficiency by normalization to the flat incoherent signal of a 1 mm water cell. The samples were held vertically in a dedicated temperature-controlled humidity chamber and aligned on a manual 4-axis goniometer head (Huber, Rimsting, Germany) embedded in the humidity chamber. The chamber was mounted on the sample rotation stage, where the lipid multilayer stacks were

scanned by rocking the wafers horizontally. The sample temperature in the chamber was maintained at 25°C during the measurements, and the humidity was varied by changing the temperature of the liquid reservoir generating the water vapor from 10°C to 24°C, leading to relative humidities ranging from to 10% to 94%. Each sample was investigated from low to high hydration by increasing the humidity step by step without opening the chamber at any time during the humidity scan. After each change in relative humidity, the sample is equilibrated between 30 min to 2 h, where equilibration is followed through the evolution of the (100) diffraction peak position in time. Equilibration time was considered to be long enough when the peak position reached a plateau. After equilibration, the rocking curve (omega scan between -1° and 8° with 0.05°) was recorded.

Results and discussion

The functional glucolipid GC18:0 is obtained by hydrogenation[31] of the monounsaturated GC18:1 compound, produced by fermentation of glucose and fatty acids by the yeast *S. bombicola ΔugtB1*.[37,38] The phase behaviour of this compound in water below concentrations of 10 wt% depends on pH and it was shown that it undergoes a micellar-to-lamellar transition at room temperature when pH is decreased from 10 to 5.[30–32] We have previously shown by small angle X-ray scattering that the membranes at acidic pH are composed of interdigitated GC18:0 molecules containing a mixture of COOH and COO^- groups and of overall thickness of about 3.6 nm.[30–32] GC18:0 solutions at pH between 6 and 7 and ionic strength between 10 and 100 mM are highly viscous, possibly gels, with shear-thinning properties.[32] A typical GC18:0 bulk solution at concentration of 1 wt% is used in this study.

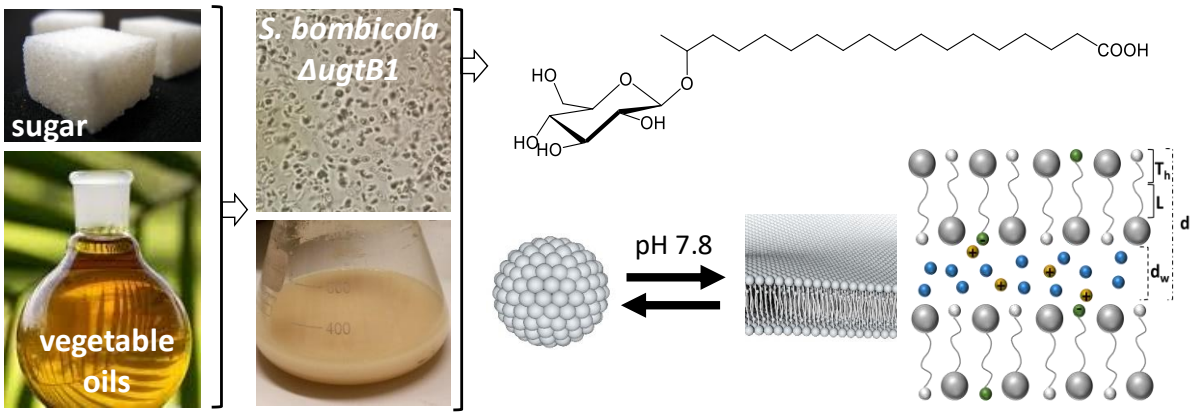

Figure 1 : Molecular structure of bolaform glucolipid GC18:0: headgroup is composed of D-glucose and the backbone is composed of a C18:0 fatty acid, with a free COOH group at the opposite end of the glucose moiety. GC18:0 is obatined by hydrogenation of the corresponding GC18:1 compound obtained by

fermentation of sugar and vegetable oil with the yeast *S. bombicola ΔugtB1*. The GC18:0 lipid undergoes a micelles-to-lamellar phase transition and the latter is formed of interdigitated GC18:0 molecules.

The GC18:0 solution, prepared in D_2O to enhance the contrast with neutrons, is drop-cast and allowed to dry on a silicon wafer, while the lamellar spacing is probed using neutron diffraction in a θ-2θ configuration, with the relative humidity ($RH\%$) varying between 98% and 10% (Figure 2a). The repeating lamellar period, $d_{(100)}$, is traced against relative humidity, $d_{(100)}(RH\%)$ (Figure 2b), and eventually converted into a $\Pi(d_{(100)})$ relationship (Figure 2b) using the following expression equalizing pressure and $RH\%$,[8]

$$\Pi = -\left(\frac{k_b T}{V_w}\right) ln\left(\frac{RH\%}{100}\right) \qquad \text{Eq. 1}$$

with Π being the osmotic pressure, k_b the Boltzmann's constant, T the temperature in degrees Kelvin, V_w the water molar volume and $RH\%$ the relative humidity. The thickness of the interlamellar water layer, d_w, is commonly obtained by subtracting the membrane thickness from $d_{(100)}$. Under high humidity conditions, above 80%, the (100) reflection settles at about 2θ= 4°, corresponding to $d_{(100)}$ of about 6 nm, while below 50%, the (100) reflection shifts towards 2θ= 6°, corresponding to $d_{(100)}$ between 4.1 and 4.5 nm. The $d_{(100)}(RH\%)$ profiles in Figure 2b show that salt has no influence in the d-spacing values at relative humidity below 40%. On the contrary, an important mismatch in d-spacing values between the 16 mM and 100 mM system occurs above $RH\%$= 40%, where $d_{(100)}$ is larger at lower salt concentration. These data confirm the trend observed in bulk for the same material by mean of neutron scattering,[32] and where the interlamellar spacing was found to vary from 22 nm to 10 nm when salt concentration increases from 50 mM to about 300 mM. Similar trends were also found for other lipid lamellar phases by when increasing salt concentration.[39,40]

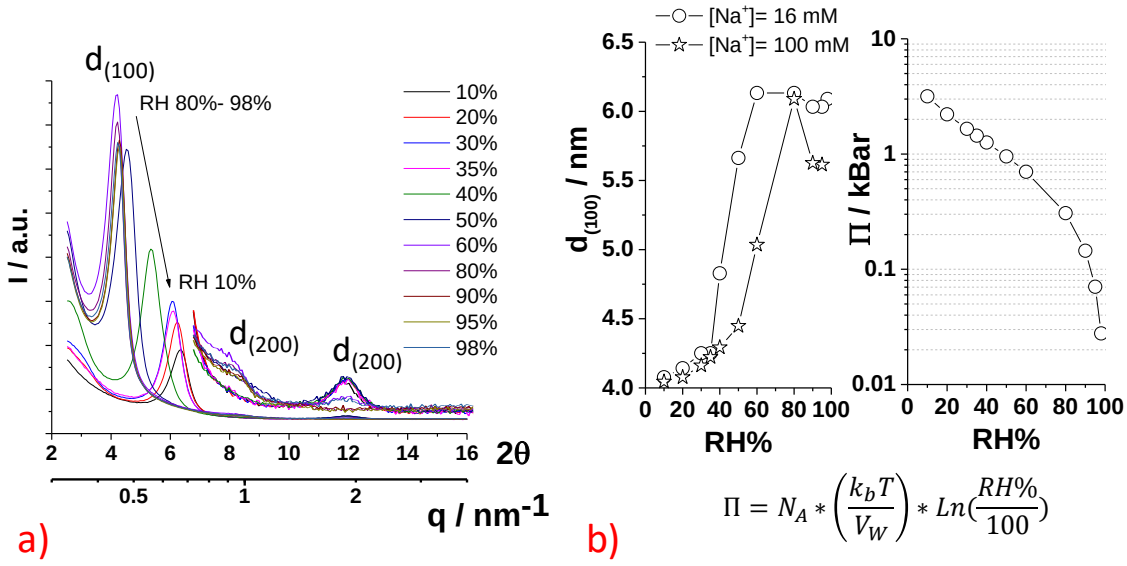

Figure 2: a) Evolution of the neutron diffraction patterns as a function of relative humidity, $RH\%$, measured on a GC18:0 solution (bulk data: C= 1 wt%, pH 6.2 ± 0.3, [NaCl]= 16 mM) drop-cast on a silicon (111) substrate. b) Evolution of the $d_{(100)}$-spacing with $RH\%$, and plot of the corresponding $\Pi(RH\%)$ relationship with N_A being the Avogadro's number, K_b the Boltzmann constant, T the temperature in Kelvin degrees and V_m the water molar volume.

In order to establish a pressure-distance, $\Pi(d_w)$, relationship, $d_{(100)}$ must be converted into the thickness of the water layer between the lamellae, d_w, by mean of Eq. 2, where 3.6 nm is the thickness of the interdigitated layer of GC18:0 measured by SAXS at concentrations below 10 wt%.[30–32] The interaction terms contained in the expression of $\Pi(d_w)$, also known as the equation of state of the lamellar system, are shown in Eq. 3 and it contains both attractive (Van der Waals, *VdW*) and repulsive (steric, hydration, electrostatic, entropic, respectively *St*, *Hyd*, *El* and *Entr*) contributions.

$$d_w(RH\%) = d_{(100)}(RH\%) - 3.6\,nm \qquad \text{Eq. 2}$$

$$\Pi(d_w) = \Pi_{VdW} + \Pi_{St} + \Pi_{Hyd} + \Pi_{El} + \Pi_{Entr} \qquad \text{Eq. 3}$$

The lin-lin plot (Figure 3a) of the $\Pi(d_w)$ curves suggests a double exponential decay, confirmed by the log-lin plots in Figure 3b-d and where the frontier between the two regimes is at 4.2 nm < $d_{(100)}$ < 4.5 nm (0.5 nm < d_w < 0.7 nm). The pressure below which the interlamellar distance is constant is generally referred to the disjoining pressure, it is commonly observed in osmotic stress experiments for water thicknesses above 2-3 nm and it can be described by the necessary

force to overcome hydration forces.[16,21,41] In the present system, the disjoining pressure is set at about 1 kbar and identified by the grey symbols at about 2.5 nm in Figure 3b-d. Hydration forces are generally found at interlamellar distances below 1 nm and they are characterized by a single exponential decay with a decay length, λ, between 0.2 – 0.4 nm.[9,11,41] In the same range of d_w, one can measure repulsive steric forces, corresponding to excluded volume steric interactions between polar groups, and with characteristic decay lengths smaller than 0.2 nm.[16] A crude double exponential fit of the $\Pi(d_{(100)})$ curves in Figure 3d yields $\lambda_1 \sim 0.3$ nm and $\lambda_2 \sim 2$ nm. If λ_1 is compatible with typical hydration decay lengths, λ_2 is excessively larger and cannot be explained with classical short-range repulsion forces (steric and hydration). At the same time, the pressure range of (1 ±0.5) kbar reached between 1 and 2 nm is also excessively high for classical long-range forces such as electrostatic or entropic.[33,42] Tentative calculations of $\Pi_{El}(d_w)$ for d_w above 0.7 nm and for any pressure regime identified in ref. [5] yields values below 1 bar, that is three orders of magnitude smaller than what we experimentally measure here. Similar values are obtained for Π_{Entr} calculated using the classical Helfrich formula[15,43] using typical bending modulus values in the order of 10-20 k_BT. In both cases, the calculated values for the pressure for $d_w > 0.7$ nm are at least 2 orders of magnitude smaller than what we find experimentally in Figure 3, as also shown in [44].

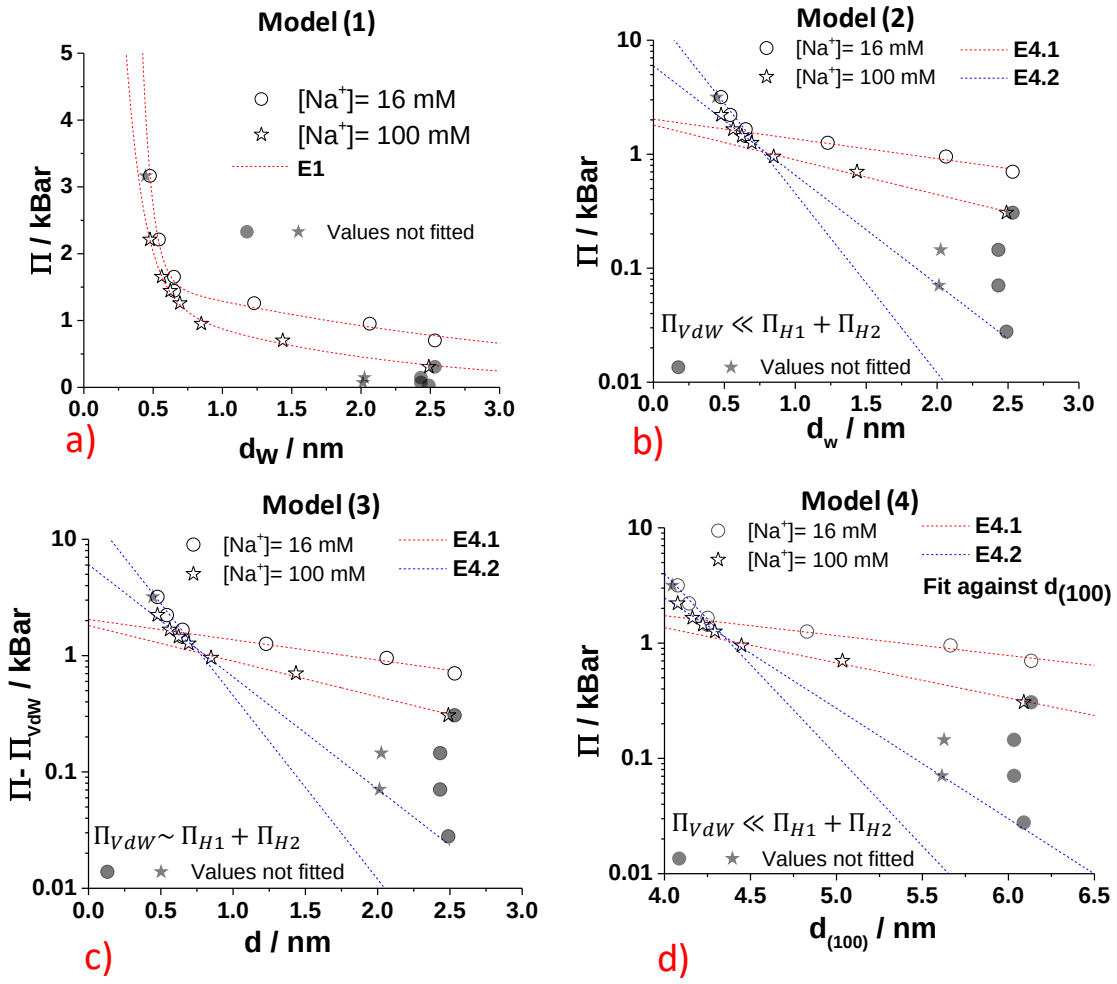

Figure 3: a-b) Various representations of the pressure-distance plots derived from the osmotic stress experiments in b). Models (1) through (4) are respectively used to fit panels c) – f). Grey-filled values identify the disjoining pressure and they are not included in the fits.

The considerations above show that if the $\Pi_{St}, \Pi_{El}, \Pi_{Entr}$ terms of can be neglected against Π_{Hyd}, one term accounting for the pressures at d_w > 0.7 nm is most likely missing, and its nature is exponential. Described long ago,[10,22,45] secondary hydration forces are commonly observed in charged lamellar systems in the presence of an electrolyte, and the typical reported λ is contained between 1 and 3 nm,[10,13,21,22,41,44,45] values which are in perfect agreement with λ_2 measured in this system. Long-range hydration forces are commonly accepted as deriving from short-range repulsion due to ion exclusion from a surface hydration layer, and longer range repulsion arising due to ionic dispersion interactions. In all cases, they have been clearly identified in lamellar systems at salt concentrations from the mM to the M range. In the systems in Figure 3, we study two concentrations of NaCl, 16 mM and 100 mM in bulk gel. $d_{(100)}$ in the gel prior to its use in the humidity chamber (or in the ice-templating device) is ~20 nm.[32]

After partial dehydration in the humidity chamber, $d_{(100)}$ ~4 nm, a factor five in shrinking and corresponding to a five-fold increase in the initial NaCl concentration. The final estimated [NaCl] in the interlamellar volume after dehydration varies between 80 mM and 500 mM, which are high enough to expect secondary hydration forces.[21,41,44] Under these circumstances, Eq. 3 can be simplified to Eq. 4, where the steric, electrostatic and entropic terms can be neglected while a second hydration term is introduced.

$$\Pi(d_w) = \Pi_{VdW} + \Pi_{Hyd1} + \Pi_{Hyd2} \qquad \text{Eq. 4}$$

Pressure-distance plots have been fitted using four different models. The discussion below presents each model separately, giving the advantages and disadvantages, and to establish an average value of the strength and length on the hydration interactions, we present and use of all of them.

Model (1). This model uses equation Eq. 4 to fit the $\Pi(d_w)$, where the expressions of Π_{VdW} is given in Eq. 5, while the primary and secondary hydration components, Π_{Hyd1} and Π_{Hyd2}, of the hydration pressure (Eq. 6, linearized in Eq. 7) are given in Eq. 8 and Eq. 9, respectively. Model (1) is the most rigorous approach, but, in order to reduce the number of terms in the fit to only four (Π_{H1}, Π_{H2}, λ_{H1}, λ_{H2}), it supposes to calculate the Π_{VdW} term. To do so, one must calculate the Hamaker constant, H, but also a good estimation of T_h and L, respectively the thickness of the hydrophilic and length of the hydrophobic regions of the membrane, and to assume that the value of 3.6 nm, used to calculate d_w, for the bilayer thickness is also a good estimation. At room temperature, these parameters can either be calculated or measured. The Hamaker constant was calculated for a generic lipid bilayer to be H= 5.1·10^{-21} J at room temperature,[46] the structural parameters of the GC18:0 interdigitated layer (IL) were estimated from the fit of SAXS data[30–32] and were assumed here to be T_h= 1.3 nm, L= 0.8 nm and the total thickness, ($2T_h$+L)= 3.6 nm. In summary, model (1) is the most rigorous but it is based on the hypothesis that variations in the Van der Waals terms of the pressure are negligible across the temperature range explored in this work.

$$\Pi_{VdW} = \frac{H}{6\pi}\left(\frac{1}{d_w^3} - \frac{2}{(d_w(RH\%) + 2T_h + L)^3} + \frac{1}{\left(d_w(RH\%) + 2(T_h + L)\right)^3}\right) \qquad \text{Eq. 5}$$

$$\Pi(d_w)_{Hyd} = \Pi_{\mathrm{H}} e^{-\frac{d_w(RH\%)}{\lambda_H}} \qquad \text{Eq. 6}$$

$$Log(\Pi_{Hyd}) = \mathrm{Log}(\Pi_{\mathrm{H}}) - \frac{0.434}{\lambda_H} d_w(RH\%) \quad \text{Eq. 7}$$

$$\Pi(d_w)_{Hyd1} = \Pi_{\mathrm{H1}} e^{-\frac{d_W(RH\%)}{\lambda_{H1}}} \quad ; d_w < 0.74 \pm 0.11\, nm \quad \text{Eq. 8}$$

$$\Pi(d_w)_{Hyd2} = \Pi_{\mathrm{H2}} e^{-\frac{d_W(RH\%)}{\lambda_{H2}}} \quad ; d_w > 0.74 \pm 0.11\, nm \quad \text{Eq. 9}$$

Model (2). In model (2), we make the hypothesis that the contribution of the Van der Waals term is negligible across the entire d_w range and the hydration terms, that is $\Pi_{VdW} << \Pi_{\mathrm{Hyd1}} + \Pi_{\mathrm{Hyd2}}$ in Eq. 4. This hypothesis holds for a system that does not follow the DLVO theory at small water thickness, as this seems to be the case for lamellar lipid phases dominated by two hydration regimes.[44] Under this hypothesis, one can represent the pressure-distance curves in a log-lin plot (Figure 3b), and in particular the hydration component (Eq. 6) can be linearized into Eq. 7. If the two hydration regimes are distinct enough, one can independently fit the short- and long-distance domains of the pressure-distance curves with equations Eq. 8 and Eq. 9 and extract the four parameters (Π_{H1}, Π_{H2}, λ_{H1}, λ_{H2}), as this was classically done in lamellar systems governed by two hydration regimes.[10,13,22]

Model (3). In model (3) we employed exactly the same approach as in model (2), but the Van der Waals contribution is not neglected anymore: Π_{VdW} is calculated exactly as in model (1) and subtracted to $\Pi(d_w)$. The resulting term is plotted against d_w in a log-lin scale (Figure 3c) and the (Π_{H1}, Π_{H2}, λ_{H1}, λ_{H2}) terms are extracted from linear fits according to equations Eq. 8 and Eq. 9. This approach, to which the attractive DLVO contribution is accurately subtracted, was classically used by Pashley in the early studies of the double hydration regime.[10,13,22] Model (3) is analogous to model (1), except for the mathematical treatment, which is simplified in model (3).

Model (4). The drawback of models (1)-(3) is the plot of the pressure against the water thickness, d_w, being calculated using equation Eq. 2 and supposing a good estimate for the membrane thickness. We use the value of 3.6 nm determined by modelling SAXS profiles in bulk, but it is well-known that fitting of SAXS curves generally requires more than one free variable and acceptable fitting can occur with more than one set of variable. Although we believe that a membrane thickness of 3.6 nm is the best estimate, one must consider an error of

least ± 0.2 nm, which may have a strong impact on the pressure-distance profiles at low relative humidity, when it becomes comparable with the value of d_w. In model (4), pressure data are plot in a log-lin representation against the interlamellar distance, $d_{(100)}$, (Figure 3d) and then assume that (Π_{H1}, Π_{H2}, λ_{H1}, λ_{H2}) are simply extracted from a double linear fit according to equations Eq. 8 and Eq. 9. One should note that we have neglected the Van der Waals contribution, as in model (2), and that in model (4) only the slopes, then λ_{H1}, λ_{H2}, are significant, while the pressure values at the intercept, Π_{H1}, Π_{H2}, are not.

Table 1: Values of the hydration pressure (Π_H) and decay lengths (λ_H) in the primary and secondary hydration regimes. Data are obtained from the fit of the osmotic stress experiments in Figure 3a-d applying models (1)-(4) to the low- (16 mM) and high-salt (100 mM) regimes. Assumptions: Model (1) : parameters for Π_{VdW} (Eq. 5): H = 5.1·10^{-21} J; T_h= 1.4·nm; L= 0.8·nm. Model (2) : $\Pi(d_w[RH\%]) - \Pi_{VdW}$ with $\Pi_{VdW} \ll \Pi_{Hyd1}; \Pi_{Hyd2}$; Model (3) : $\Pi(d_w[RH\%]) - \Pi_{VdW}$ with $\Pi_{VdW} \sim \Pi_{Hyd1}; \Pi_{Hyd2}$; Model (4) : $\Pi(d_{(100)}[RH\%]) - \Pi_{VdW}$ with $\Pi_{VdW} \ll \Pi_{Hyd1}; \Pi_{Hyd2}$. This model if fit against $d_{(100)}[RH\%]$

Model N°	Method	Equation	[Na$^+$] / mM	Π_{H1}/kbar	λ_{H1}/nm	Π_{H2}/kbar	λ_{H2}/nm
(1)	Fit (Lin-Lin)	Eq. 4	16	1.26·10^3	0.07 ± 20%	1.81	2.98 ± 20%
			100	37.5	0.13 ± 10%	1.61	1.59 ± 10%
(2)	Linear fit (Log-Lin)	Eq. 8	16	17.0 ± 40%	0.28 ± 20%	2.04 ± 15%	2.53 ± 20%
		Eq. 9	100	5.94 ± 7%	0.45 ± 10%	1.80 ± 12%	1.43 ± 10%
(3)	Linear fit (Log-Lin)	Eq. 8	16	17.3 ± 40%	0.28 ± 20%	2.04 ± 15%	2.50 ± 20%
		Eq. 9	100	6.05 ± 7%	0.45 ± 10%	1.81 ± 2%	1.42 ± 10%
(4)	Linear fit (Log-Lin)	Eq. 8	16	7.93·10^6	0.28 ± 20%	8.47	2.52 ± 20%
		Eq. 9	100	1.66·10^4	0.45 ± 10%	8.47	1.42 ± 10%
	Average all				**0.29 ± 0.15**		**2.05 ± 0.64**
	Average (Fit Log-lin)				**0.37 ± 0.12**		**1.97 ± 0.78**

Table 1 summarizes the (Π_{H1}, Π_{H2}, λ_{H1}, λ_{H2}) parameters obtained from the application of models (1)-(4) on the pressure-distance curves obtained from the humidity chamber experiments performed on two GC18:0 (C = 1 wt%, pH = 6.3 ± 0.3) lamellar hydrogel samples at salt concentrations in the gel (prior to deposition onto the sample holder), [NaCl] = 16 mM and 100 mM. The following observations must be done:

a) *Agreement between our values and literature*. The values of λ_{H1} and λ_{H2}, averaged over all models, are respectively 0.29 ± 0.15 and 2.05 ± 0.64. These values, despite

the error (discussed here below) are characteristics for the short- and long-range decay lengths found in lamellar lipid systems characterized by primary and secondary hydration:[21,44] the values of the decay lengths are not dependent of the model used.

b) *Impact of the model*. Hydration forces are known to be very sensitive to salt concentration, and for this reason we run two experiments at [NaCl] = 16 mM and 100 mM. These values are the "bulk" values, and one should consider a five-fold increase in concentration in the humidity chamber, as already commented above. When using models (2)-(4), λ_{H1} and λ_{H2} are highly homogeneous at each salt concentration, e.g., λ_{H1}= 0.28 nm and λ_{H2}= 2.52 nm at [NaCl] = 16 mM. On the contrary, model (1) provides values of the decay length λ_{H1}, which are smaller by a factor three in the short range hydration respect to the values obtained using models (2)-(4). Estimation of the longer decay lengths λ_{H2} are also slightly different between (1) and (2)-(4), but still comparable within the error. The poor results of model (1) are particularly visible in the values of the pressure, whereas models (2)-(3) provide Π_{H1} in the order of several kbar, while model (1) provides an exceedingly high value of 10^3 kbar, which is not realistic. The above illustrates how the large error in the average values are mainly directed by the poor estimates obtained from model (1).

c) *Impact of salt concentration*. Figure 3a-d show that salt has little influence at small distances (typically below water thickness of 0.7 nm), where the data at 16 mM and 100 mM are practically superimposed. Nonetheless, the limited number of experimental points recorded provide two distinct values of λ_{H1}, respectively 0.28 nm at 16 mM and 0.45 nm at 100 mM (analysis is here limited to models (2)-(4) only). Nonetheless, these values are still comparable within the error, providing an average λ_{H1}= (0.37 ± 0.12) nm. This value and its small dependence on salt concentration are both in strong agreement with primary hydration forces, generally related to enthalpic adsorption energy of water layers.[21,41,44] When it comes to secondary hydration at larger distances, Figure 3a-d show a strong impact of the initial salt concentration on the pressure-distance profiles. The corresponding decay length, λ_{H2}, are in worst agreement among themselves λ_{H2}= (1.97 ± 0.78) nm, with a relative error of about 40%, and they highlight the strong impact of salt. These aspects are in agreement with the literature data on secondary

hydration,[10,13,21,22,41,44,45] of which the origin was attributed to the competition between water bound to the counterions and water bound to the bilayer surface.[41]

Conclusion.

We have used four models to fit the pressure-distance curves of the GC18:0 lamellar phase. We have explored the short-range regime at water thicknesses below 3 nm. This regime is nicely probed by the humidity chamber apparatus and we have tested two different salt concentrations, a low-salt ([NaCl]= 16 mM) and a high-salt ([NaCl]= 100 mM) regime. These concentrations are intended to in the bulk system, before deposition on the sample holder, after which the local salt concentration experience up to a five-fold increase in between the lamellar domains. The experimental data are nicely modeled using a double exponential, rendering the primary and secondary hydration, the latter due to the hydration of the counterions. Whichever model is used, the interdigitated layers in the sample experience two hydration regimes with decay lengths at about 0.3 nm and 2 nm, as expected from the literature. Both the choice of the model, the amount of salt and the limited number of points generate an expected, although mild, dispersion in the hydration pressures and decay lengths. Alltogether the models provide a consistent set of data for both the primary and secondary hydration regions. Furthermore, exploring the low-salt and high-salt regimes allow us to take into account the same GC18:0 gels used in the ice-templating device.

Acknowledgements

We thank Dr. S. Roelants and Prof. Wim Soetaert (Gent University, Belgium) for producing the GC18:0 compound and Dr. E. Delbeke and Prof. C. Stevens (Gent University, Belgium) for the hydrogenation reaction. Access to the D16 beamline was financed by ILL under the proposal number 9-13-783.

References

1. Steiner, A. *et al.* Entropic attraction condenses like-charged interfaces composed of self-assembled molecules. *Langmuir* **28**, 2604–2613 (2012).
2. Richter, R. P., Bérat, R. & Brisson, A. R. Formation of solid-supported lipid bilayers: An integrated view. *Langmuir* **22**, 3497–3505 (2006).
3. Wessman, P., Strömstedt, A. A., Malmsten, M. & Edwards, K. Melittin-lipid bilayer interactions and the role of cholesterol. *Biophys. J.* **95**, 4324–4336 (2008).
4. Kanduč, M. *et al.* Tight cohesion between glycolipid membranes results from balanced

water–headgroup interactions. *Nat. Commun.* **8**, 14899 (2017).

5. Markovich, T., Andelman, D. & Podgornik, R. Charged Membranes: Poisson-Boltzmann theory, DLVO paradigm and beyond. in *Handbook of lipid membranes* 3 (2016).

6. Petrache, H. I., Zemb, T., Belloni, L. & Parsegian, V. A. Salt screening and specific ion adsorption determine neutral-lipid membrane interactions. *Proc. Natl. Acad. Sci.* **103**, 7982–7987 (2006).

7. Mcintosh, T. J., Magid, A. D. & Simon, S. A. Cholesterol Modifies the Short-Range Repulsive Interactions between Phosphatidylcholine Membranes. *Biochemistry* **28**, 17–25 (1989).

8. Ricoul, F. *et al.* Phase Equilibria and Equation of State of a Mixed Cationic Surfactant-Glycolipid Lamellar System. *Langmuir* **14**, 2645–2655 (1998).

9. Leikin, S., Parsegian, V. A., Rau, D. C. & Rand, R. P. Hydration Forces. *Annu. Rev. Phys. Chem.* **44**, 369–395 (1993).

10. Pashley, R. M. & Quirk, J. P. The Effect of Cation Valency on DLVO and Hydration Forces between Macroscopic Sheets of Muscovite Mica in Relation to Clay Swelling. *Colloids and Surfaces* **9**, 1–17 (1984).

11. McIntosh, T. J. & Simon, S. A. Hydration and Steric Pressures between Phospholipid Bilayers. *Annu. Rev. Biophys. Biomol. Struct.* **23**, 27–51 (1994).

12. Israelachvili, J. *Intermolecular and Surface Forces*. *Intermolecular and Surface Forces* (Academic Press, 2011). doi:10.1016/C2009-0-21560-1

13. Pashley, R. M. & Israelachvili, J. N. DLVO and Hydration Forces between Mica Surfaces in. *J. Colloid Interface Sci.* **97**, (1984).

14. Caillé, A. Remarques sur la diffusion de rayons X dans les smectiques A. *C. R. Hebd. Acad. Sci. Paris B* **274**, 891 (1972).

15. Helfrich, W. Steric Interaction of Fluid Membranes in Multilayer Systems. *Z. Naturforsch* **33a**, 305–315 (1978).

16. Rand, R. P. & Parsegian, V. A. Hydration forces between phospholipid bilayers. *BBA - Rev. Biomembr.* **988**, 351–376 (1989).

17. Brotons, G. *et al.* The role of counterions on the elasticity of highly charged lamellar phases: A small-angle x-ray and neutron-scattering determination. *J. Chem. Phys.* **123**, 024704 (2005).

18. Fink, L. *et al.* Osmotic Stress Induced Desorption of Calcium Ions from Dipolar Lipid Membranes. *Langmuir* **33**, 5636–5641 (2017).

19. Marčelja, S. Hydration forces near charged interfaces in terms of effective ion potentials. *Curr. Opin. Colloid Interface Sci.* **16**, 579–583 (2011).

20. Demé, B. & Zemb, T. Hydration forces between bilayers in the presence of dissolved or surface-linked sugars. *Curr. Opin. Colloid Interface Sci.* **16**, 584–591 (2011).

21. Kralchevsky, P. A., Danov, K. D. & Basheva, E. S. Hydration force due to the reduced screening of the electrostatic repulsion in few-nanometer-thick films. *Curr. Opin.*

Colloid Interface Sci. **16**, 517–524 (2011).

22. Pashley, R. M. Hydration Forces Betmeen Mca Surfaces in Electrolyte Solutions. *Adv. Colloid Interface Sci.* **16**, 57–62 (1982).

23. Sparr, E. & Wennerström, H. Interlamellar forces and the thermodynamic characterization of lamellar phospholipid systems. *Curr. Opin. Colloid Interface Sci.* **16**, 561–567 (2011).

24. Demé, B., Cataye, C., Block, M. A., Maréchal, E. & Jouhet, J. Contribution of galactoglycerolipids to the 3-dimensional architecture of thylakoids. *FASEB J.* **28**, 3373–3383 (2014).

25. Claesson, P. M. Interactions Between Surfaces Coated with Carbohydrates, Glycolipids, and Glycoproteins. in *Biopolymers at Interfaces, Second Edition* (ed. Malmsten, M.) 165 (CRC Press, 2003).

26. Paulino, B. N. *et al.* Current status in biotechnological production and applications of glycolipid biosurfactants. *Appl. Microbiol. Biotechnol.* **100**, 10265–10293 (2016).

27. Lang, S. Biological amphiphiles (microbial biosurfactants). *Curr. Opin. Colloid Interface Sci.* **7**, 12–20 (2002).

28. Corti, M., Cantù, L., Brocca, P. & Del Favero, E. Self-assembly in glycolipids. *Curr. Opin. Colloid Interface Sci.* **12**, 148–154 (2007).

29. Kitamoto, D., Morita, T., Fukuoka, T., Konishi, M. & Imura, T. Self-assembling properties of glycolipid biosurfactants and their potential applications. *Curr. Op. Coll. Interf. Sci.* **14**, 315–328 (2009).

30. Baccile, N. *et al.* Self-Assembly Mechanism of pH-Responsive Glycolipids: Micelles, Fibers, Vesicles, and Bilayers. *Langmuir* **32**, 10881–10894 (2016).

31. Baccile, N. *et al.* PH-Driven Self-Assembly of Acidic Microbial Glycolipids. *Langmuir* **32**, 6343–6359 (2016).

32. Ben Messaoud, G. *et al.* Single-Lipid Lamellar Hydrogels: from Gel Engineering to Soft Materials Design. *arXiv* 1907.02223 (2019).

33. Demé, B., Dubois, M. & Zemb, T. Giant collective fluctuations of charged membranes at the lamellar-to-vesicle unbinding transition. 2. Equation of state in the absence of salt. *Langmuir* **18**, 1005–1013 (2002).

34. Gonthier, J. *et al.* BerILL: The ultimate humidity chamber for neutron scattering. *J. Neutron Res.* **21**, 65–76 (2019).

35. Baccile, N. *Measuring the interbilayer pressure in glucolipids lamellar phases using a humidity chamber*. (2019). doi:0.5291/ILL-DATA.9-13-783

36. Richard, D., Ferrand, M. & Kearley, G. J. Analysis and visualisation of neutron-scattering data. *J. Neutron Res.* (1996). doi:10.1080/10238169608200065

37. Saerens, K. M. J., Zhang, J., Saey, L., Van Bogaert, I. N. A. & Soetaert, W. Cloning and functional characterization of the UDP-glucosyltransferase UgtB1 involved in sophorolipid production by Candida bombicola and creation of a glucolipid-producing yeast strain. *Yeast* **28**, 279–292 (2011).

38. Saerens, K. M. J., Roelants, S. L., Van Bogaert, I. N. & Soetaert, W. Identification of the UDP-glucosyltransferase gene UGTA1, responsible for the first glucosylation step in the sophorolipid biosynthetic pathway of Candida bombicola ATCC 22214. *FEMS Yeast Res.* **11**, 123–132 (2011).

39. Szekely, O. *et al.* The structure of ions and zwitterionic lipids regulates the charge of dipolar membranes. *Langmuir* **27**, 7419–7438 (2011).

40. Dvir, T. *et al.* Charged membranes under confinement induced by polymer-, salt-, or ionic liquid solutions. *Soft Matter* **9**, 10640 (2013).

41. Parsegian, V. A. & Zemb, T. Hydration forces: Observations, explanations, expectations, questions. *Curr. Opin. Colloid Interface Sci.* **16**, 618–624 (2011).

42. Leontidis, E., Aroti, A., Belloni, L., Dubois, M. & Zemb, T. Effects of monovalent anions of the Hofmeister series on DPPC lipid bilayers part II: Modeling the perpendicular and lateral equation-of-state. *Biophys. J.* **93**, 1591–1607 (2007).

43. Helfrich, W. & Servuss, R.-M. Undulations, Steric Interaction and Cohesion of Fluid Membranes. *Nuovo Cim.* **3**, 137–151 (1984).

44. Parsons, D. F. & Ninham, B. W. Surface charge reversal and hydration forces explained by ionic dispersion forces and surface hydration. *Colloids Surfaces A Physicochem. Eng. Asp.* **383**, 2–9 (2011).

45. Israelachvili, J. N. & Pashley, R. M. Molecular layering of water at surfaces and origin of repulsive hydration forces. *Nature* **306**, 249–250 (1983).

46. Demé, B., Dubois, M. & Zemb, T. Swelling of a lecithin lamellar phase induced by small carbohydrate solutes. *Biophys. J.* **82**, 215–225 (2002).